Engineering Structures 168 (2018) 69–81

Contents lists available at ScienceDirect

Engineering Structures

journal homepage: www.elsevier.com/locate/engstruct

Fatigue performance of orthogonally reinforced concrete slabs: Experimental investigation

C.A. Spathelf*[,1,2], T. Vogel[3]

ETH Zurich, Institute of Structural Engineering, Stefano-Franscini-Platz 5, 8093 Zurich, Switzerland

ARTICLE INFO

Keywords:
Reinforced concrete
Bridge deck slabs
Cyclic loading
Fatigue
Reinforcing steel

ABSTRACT

The fatigue performance of reinforced concrete slabs was investigated under clearly defined bending conditions with large scale tests. Two series of four tests exhibiting orthogonal reinforcement layouts at different orientations were subjected to constant force-amplitude cyclic loading. The reinforcement direction in the reference series of tests coincided with the direction of principal moment. In the second series of tests, a deviation of 45° between the principal moment and reinforcement direction was introduced. The effect of inclined reinforcing bars with respect to the principal moment direction on the fatigue strength of structural concrete slabs is described. Direct measurement of reinforcing steel strains enabled a characterisation of the redistribution of internal forces within the cross-section after failure of individual bars until global failure of the slab.

1. Introduction

The load-carrying capacity of the composite material *reinforced concrete* lies in the ability of the concrete to resist (primarily) compressive forces and of the reinforcement to resist tensile forces after cracking of the concrete. Research on reinforced concrete under the influence of fluctuating loads, however, indicates that the integrity of both materials as well as their interaction through bond [1] deteriorates under repeated loading. The *CEB* state of the art report [2] provides an insightful overview of previous work on this phenomenon of fatigue of structural concrete.

Concrete members subjected predominantly to cyclic flexural loading typically exhibit increases in the width of existing cracks through a progressive deterioration of bond; disproportionally large deflections result and failure ensues through rupture of individual reinforcing bars or spalling of the concrete in the flexural compressive zone [3]. This failure mode has been observed in numerous experimental investigations [4–6]. *Fehlmann* and *Vogel* [7] investigated the fatigue performance of a typical frame type bridge in a large-scale test with the prescribed fatigue load model according to the current Swiss standard [8]. Virtually no changes in the load-carrying response, apart from the formation of some new cracks, was observed during approximately 90% of the fatigue life. Fatigue damage to the structure remained mostly undetected by conventional methods until shortly before failure. Furthermore, some investigations have shown that concrete members subjected to cyclic loading can exhibit different failure modes to those predicted under static loading. *Chang* and *Kesler* [9] conducted a large number of tests on beams in which specimens failed in flexure under static loading and due to fatigue shear modes under cyclic loading. It is currently neither possible to establish the present state of damage in a structural concrete member, nor to predict the remaining fatigue life for future loads [7].

The deck slabs of concrete bridges have been identified to be susceptible to fatigue [10]. Slabs are in direct contact with the wheel loads of heavy vehicles and typically exhibit small ratios of own weight to live loads. A numerical investigation of the stress range in various bridge cross-sections under traffic loads indicates that particularly the transverse deck slab direction at the cantilevers and between the webs is fatigue critical in the absence of prestressing [11]. Due to the highly statically indeterminate nature of slabs and considerable capacity to redistribute stresses, loads are resisted through combinations of bending and torsional moments. Such bending action is typically resisted by layers of finely spaced reinforcing steel bars in an orthogonal layout. As a result, the direction of principal moment will deviate from the reinforcement directions under certain loading and support conditions. A scarcity of experimental data considering the fatigue performance of slabs under clearly defined combinations of bending and torsional moments prompted the tests described in the present paper.

* Corresponding author.
E-mail addresses: spathelf@alumni.ethz.ch (C.A. Spathelf), vogel@ibk.baug.ethz.ch (T. Vogel).
[1] Research associate at Institute of Structural Engineering, ETH Zurich, Switzerland.
[2] Engineer at Bigler AG Ingenieure & Planer SIA, Schwyz, Switzerland.
[3] Professor at Institute of Structural Engineering, ETH Zurich, Switzerland.

https://doi.org/10.1016/j.engstruct.2018.04.058
Received 21 December 2017; Received in revised form 4 April 2018; Accepted 16 April 2018

Nomenclature

A_{gt}	reinforcing steel strain at peak load
E_c	modulus of elasticity of concrete
E_s	modulus of elasticity of reinforcing steel
F	applied force
F_{act}	actuator force
F_{max}, F_{min}	maximum and minimum applied load during cyclic loading
G	own weight of loading yoke and rocker bearings in test setup
$M_{n,max}, M_{n,min}$	maximum and minimum bending moment in n-direction
N	number of load cycles
$N_{s,fat}$	number of load cycles corresponding to nominal fatigue strength
N_u	maximum number of load cycles to failure
R	support reactions
SG 1…SG 7	strain gauges
c_{nom}	nominal concrete cover to the reinforcement
$f_{c,cube}$	concrete cube compressive strength
f_{cc}	concrete cylinder compressive strength
f_{ct}	concrete tensile strength
$f_{su,stat}$	static tensile strength of reinforcing steel
$f_{sy,stat}$	static yield strength of reinforcing steel
g_{c0}, g_{m0}	own weight of specimens per unit length
h	height
m_1, m_2	principal moments per unit length
m_x, m_y	bending moments per unit length in the x- and y-directions
m_{xy}	torsional moment per unit length relative to x- and y-directions
u_1, u_2	concrete deformations on top surface and soffit in n-direction
w_1, w_2	midspan deflection at front and back surface of specimen
w_m	average midspan deflection
w_r	crack width
$\Delta\sigma_s$	reinforcing steel stress range
$\Delta\sigma_{s,fat}, \Delta\sigma_{sd,fat}$	nominal and design fatigue strength of reinforcing steel
ε_{cu}	concrete strain at peak load
ε_{su}	rupture strain of reinforcing steel
ε_{sv}	reinforcing steel strain at onset of strain-hardening
$\varepsilon_{sx}, \varepsilon_{sy}$	reinforcing steel strains in the x- and y-directions
ρ_x, ρ_y	geometric reinforcement content in the x- and y-directions
σ_1, σ_2	principal stresses
σ_n, σ_t	normal stresses in the n- and t-directions
σ_{sx}, σ_{sy}	reinforcing steel stress in the x- and y-directions
σ_x, σ_y	normal stresses in the x- and y-directions
φ_n	angle defining reinforcement direction
∅	diameter

An experimental campaign consisting of two series of four large-scale tests was carried out at the structural laboratory of ETH Zurich. Slab specimens were reinforced with standard profiled reinforcing steel bars in an orthogonal layout and tested under constant force-amplitude cyclic loading. Reinforcement layouts were investigated wherein (1) the principal moment and reinforcement direction coincide and (2) with the introduction of a 45° deviation between the principal moment and reinforcement directions. The primary objective was to investigate whether an inclination of reinforcing bars with respect to the principal moment/stress direction detrimentally influences the fatigue strength of reinforced concrete slabs. The redistribution of internal forces within the reinforcement after failure of individual bars was studied as well as the characterisation of development in response between fatigue failure of the first reinforcing bar and global failure of the slab.

2. Testing program

Two slab strips were constructed in each of the two series of tests with the reinforcement layouts indicated in Fig. 1. The tests of series A constituted the reference set in which only one layer of reinforcement was activated under bending action. Through a rotation of the orthogonal reinforcement layout by $\varphi_n = 45°$ with respect to the principal moment direction, both layers of reinforcement were activated in tension in the tests of series B. Specimens were subjected to a high level of constant amplitude cyclic loading in which the maximum load F_{max} resulted in a bending demand of approximately 65% of the theoretical yield moment. The minimum load F_{min} was defined such that the expected reinforcing steel stress range clearly exceeded the fatigue endurance limit of the reinforcement.

In the tests of series A, the orientation of the activated reinforcement in x-direction corresponded to the principal moment direction such that $m_x = m_1$ and $m_y = m_{xy} = 0$. In the tests of series B, the activated reinforcement in both the x- and y-directions deviated from the principal moment direction. This resulted in a combination of bending and torsional moments with respect to the reinforcement directions corresponding to $m_x = m_y = m_{xy} = 0.5 \cdot m_1$. These bending conditions are indicated graphically on Mohr's circle for bending and torsional moments in Fig. 1(c). Considering the tensile zone of each slab as an equivalent reinforced concrete membrane, see Fig. 1(b), allows a description of the corresponding stress states in the reinforcement and in the concrete between cracks as shown in Fig. 1(d). Flexural cracks in the concrete form perpendicular to the direction of the larger (tensile) principal stress. Hence, the concrete between cracks remains unstressed in the tests of series A and the principal stress at the crack is resisted exclusively by the reinforcement in x-direction such that $\sigma_1 = \sigma_{sxr} \cdot \rho_x$. Considering equilibrium at the cracks in the tests of series B indicates that the applied stress is resisted by both layers of reinforcement. The corresponding equilibrium condition results to $\sigma_1 = \sigma_{sxr} \cdot \rho_x = \sigma_{syr} \cdot \rho_y$.

3. Test specimens

The geometry and reinforcement layout of the specimens of series A and B are illustrated in Fig. 2. The test parameters, summarised in Table 1, are identical for both series with the exception of the direction of the flexural reinforcement φ_n with respect to the n-axis. Two orthogonally placed layers of reinforcement were provided in the flexural tensile zone at a spacing of 100 mm with a nominal concrete cover of $c_{nom} = 20$ mm to the reinforcement. The orientation of the outer and inner layers of reinforcement corresponded to the x- and y-directions, respectively. All reinforcing bars activated in tension were ordered with end anchorages of the type ancoFIX®, see [13], in order to ensure a short bond development length within the edge regions of the specimen. The flexural compression zone remained unreinforced. Vertical shear reinforcement was provided between the supports and the cross-sections of load application in order to prevent a premature shear failure of the concrete.

The reinforcement for the specimens of series A consisted of 8 ∅12 mm bars placed parallel to the longitudinal or n-axis of the specimen in the outer layer with 26 ∅12 mm bars constituting the inner layer in the transverse direction (t-axis). The flexural reinforcement in the specimens of series B consisted of two layers of 22 ∅12 mm bars each, which were placed with deviations of −45° and 45° with respect to the specimen n-axis. An approximately isotropic reinforcement layout resulted in all specimens with geometric reinforcement contents of

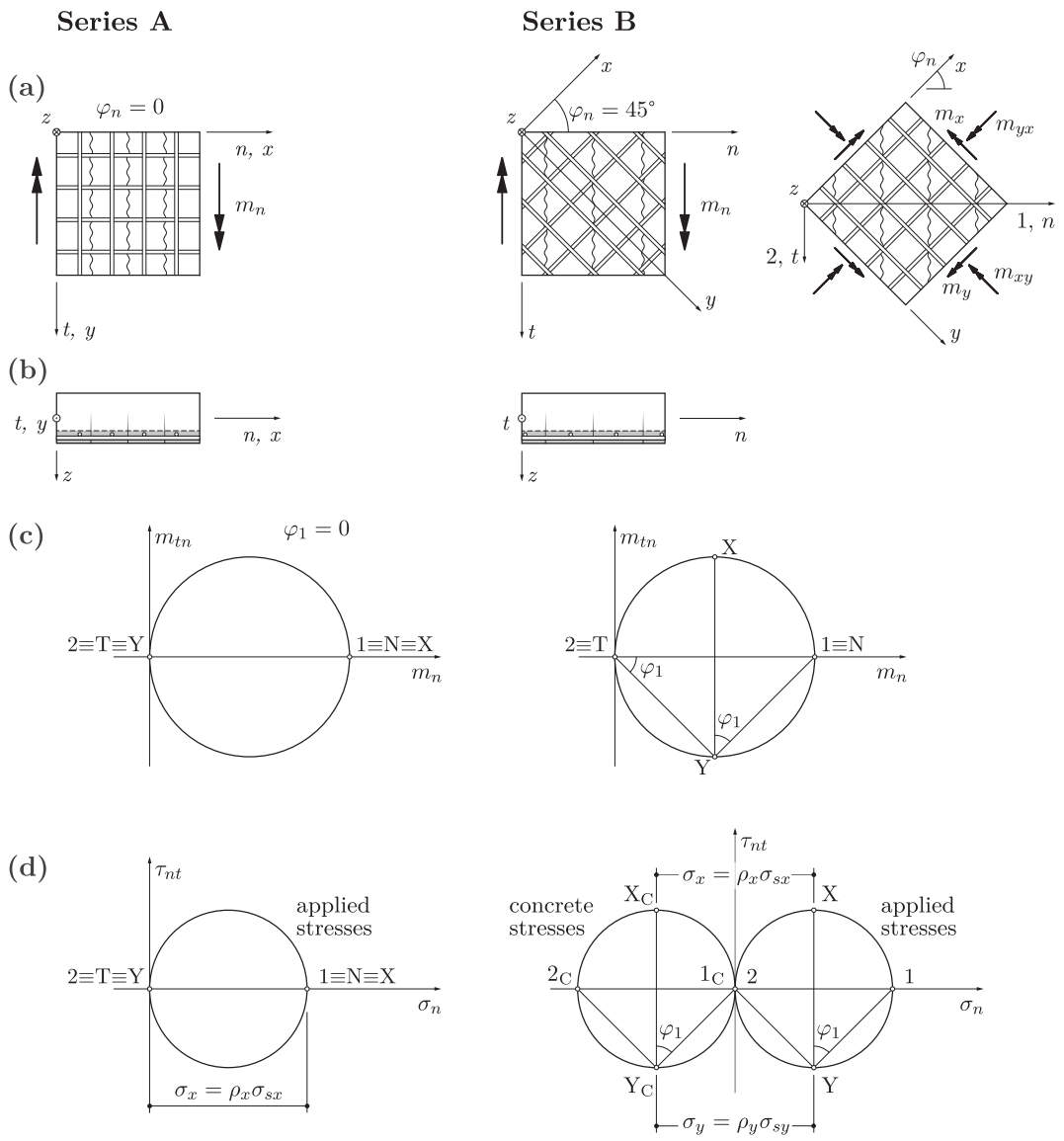

Fig. 1. Overview of testing program: (a) plan views with notation; (b) cross-sectional views; (c) Mohr's circle for bending and torsional moments; (d) stress state of equivalent membrane cover elements. Representation adapted from [12].

$\rho_x = 0.65\%$ and $\rho_y = 0.70\%$ for the x- and y-directions, respectively.

All test specimens were produced with the same concrete mix. The mechanical properties of the concrete were determined by testing a total of 20 cylinders ($\varnothing = 150$ mm,$h = 300$ mm) and 12 cubes (side lengths 150 mm). The concrete compressive strength and the modulus of elasticity were determined by testing all 12 cubes and 12 of the cylinders. The remaining eight cylinders were cut in half and used to determine the splitting tensile strength in double-punch tests. Concrete material tests were performed prior to the testing of each specimen in order to record the development of concrete strength with increasing age. The mechanical properties of the concrete is summarised in Table 2.

Standard profiled steel bars with a nominal diameter of 12 mm were used for the flexural reinforcement in all four specimens. All steel bars were procured from the same heat in order to ensure uniform material properties with respect to chemical composition and manufacturing conditions. The mechanical properties of the steel were determined by direct tensile tests on 15 bars randomly selected from the batch. All strengths were calculated considering the nominal bar diameter. A summary of the mechanical properties of the reinforcing steel is provided in Table 3.

4. Test procedure

4.1. Test setup

The test setup used for all four tests is illustrated in Fig. 3. A steel frame was constructed and prestressed to the strong floor as a reaction structure for a centrally placed servo-hydraulic actuator. A loading yoke, consisting of a load-transfer beam and two spreader-beams, enabled a uniform distribution of the applied force across the specimen width at two load application cross-sections. The force was applied on the top surface of the specimen through two rocker bearings at a spacing of 1.12 m. The specimen was supported over a span of 2.40 m on two rocker bearings; one of which was bolted to the supporting structure, whilst the other was mounted on a steel-Teflon sliding surface that enabled translation in the longitudinal direction. The supports constituted statically determinate boundary conditions, ensuring that the sectional forces could be kept constant for the duration of the test as they depended only on the setup geometry and the applied load.

Cyclic loading was applied under displacement control using a triangular loading protocol. The rate of change in applied force varied according to the specimen stiffness, thus resulting in slightly different

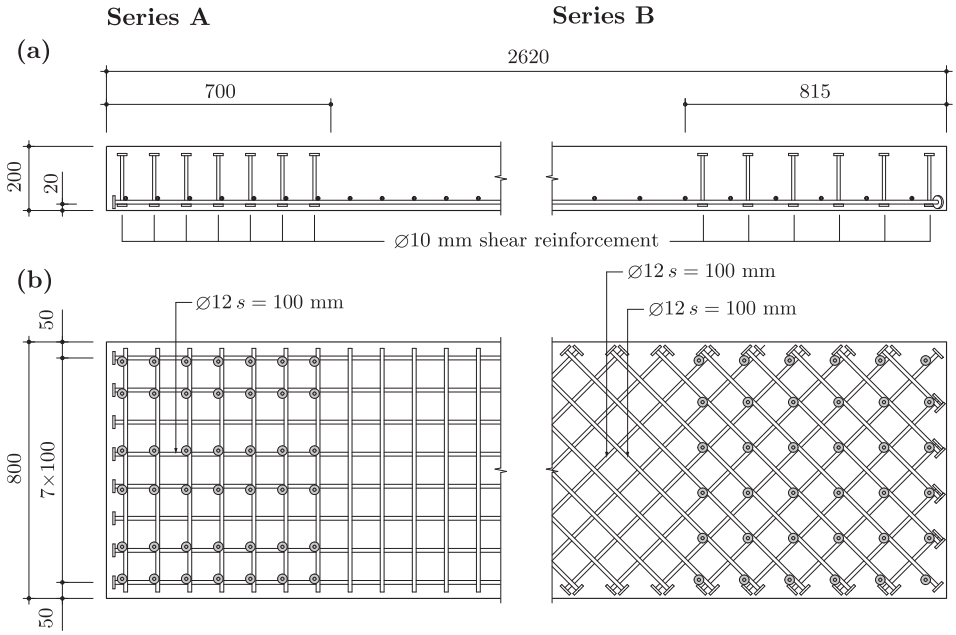

Fig. 2. Geometry and reinforcement: (a) side view; (b) plan view. Dimensions in mm.

Table 1
Test parameters.

Series			A	B
Slab thickness	h	[mm]	200	200
Reinforcement direction	φ_n	[°]	0	45
Reinforcement content in x-direction	ρ_x	[%]	0.65	0.65
Reinforcement content in y-direction	ρ_y	[%]	0.70	0.70
Moment at maximum load	$M_{n,\max}$	[kN m]	46.64	46.64
Moment at minimum load	$M_{n,\min}$	[kN m]	12.80	12.80

loading frequencies as increasing damage led to larger displacements. The average loading frequencies changed from 1.0 and 0.7 Hz during the initial load cycles to 0.7 and 0.6 Hz shortly before failure in the tests of series A and B respectively. The average test duration including periods of manual measurements in which the cyclic loading was interrupted amounted to approximately 9 weeks.

4.2. Measurements

Manual measurements were made during the initial loading and periodically at maximum and minimum load between intervals of cyclic loading. These measurements included: (i) recording local concrete deformations on all surfaces of the specimen as well as measuring the slab deflection with demountable deformeters, (ii) marking newly formed concrete cracks and recording crack widths, (iii) photographing the specimen, and (iv) nondestructive detection of damage to the reinforcement. A newly developed approach for damage detection in ferromagnetic reinforcement through the measurement and interpretation of constant magnetic fields, namely, the *magnetic flux leakage method*, was used to detect fractures in the reinforcement.

Continuous measurements of the applied force, midspan deflection, concrete deformations on the top surface and soffit as well as reinforcing steel strains were made with 15 permanently installed sensors, see Fig. 4. The applied actuator force F_{act} was recorded with a load cell integrated into the actuator housing. The slab midspan deflection was measured with a Linear Variable Displacement Transformer (LVDT) at the front w_1 and at the back surface w_2 of the specimen. Concrete deformations within the constant moment region were measured on the top surface u_1 and soffit u_2 with LVDTs over a base length of 350 mm. Reinforcing steel strains were measured with six strain gauges SG 1–SG 6 applied directly to two bars in each specimen. The instrumented bars were milled along the longitudinal rib at these locations in order to produce even, flat surfaces on which the strain gauges were glued, see Fig. 5. This preparation of the bars resulted in localised cross-sectional reductions of approximately 4%. Each strain gauge was subsequently coated with a silicone gel for insulation from moisture and mechanical protection. In addition, the influence of temperature fluctuations on the

Table 3
Mechanical properties of reinforcing steel; mean values with coefficient of variation.

Static yield strength	$f_{sy,\text{stat}}$	[N/mm^2]	554.6 ± 1.5%
Static ultimate strength	$f_{su,\text{stat}}$	[N/mm^2]	612.5 ± 2.2%
Strain at onset of strain-hardening	ε_{sv}	[‰]	30.1 ± 2.2%
Strain at peak load	A_{gt}	[‰]	91.6 ± 6.5%
Ultimate strain	ε_{su}	[‰]	112.6 ± 8.8%
Modulus of elasticity	E_s	[kN/mm^2]	201.3 ± 1.4%

Table 2
Mechanical properties of concrete; mean values with coefficient of variation.

Specimen		A1	A2	B1	B2
Age of concrete	[d]	96	343	209	384
Cube compressive strength, $f_{c,\text{cube}}$	[N/mm^2]	51.8 ± 6.3%	56.4 ± 3.5%	56.9 ± 6.3%	55.6 ± 3.3%
Cylinder compressive strength, f_{cc}	[N/mm^2]	51.3 ± 2.5%	51.9 ± 0.8%	52.1 ± 6.9%	51.9 ± 4.4%
Splitting tensile strength, f_{ct}	[N/mm^2]	3.92 ± 5.3%	3.61 ± 6.1%	3.59 ± 5.7%	3.67 ± 10.1%
Strain at peak load, ε_{cu}	[‰]	2.51 ± 1.4%	2.35 ± 0.2%	2.32 ± 9.8%	2.34 ± 3.2%
Modulus of elasticity, E_c	[kN/mm^2]	34.9 ± 2.0%	34.7 ± 1.2%	34.5 ± 1.2%	34.1 ± 1.0%

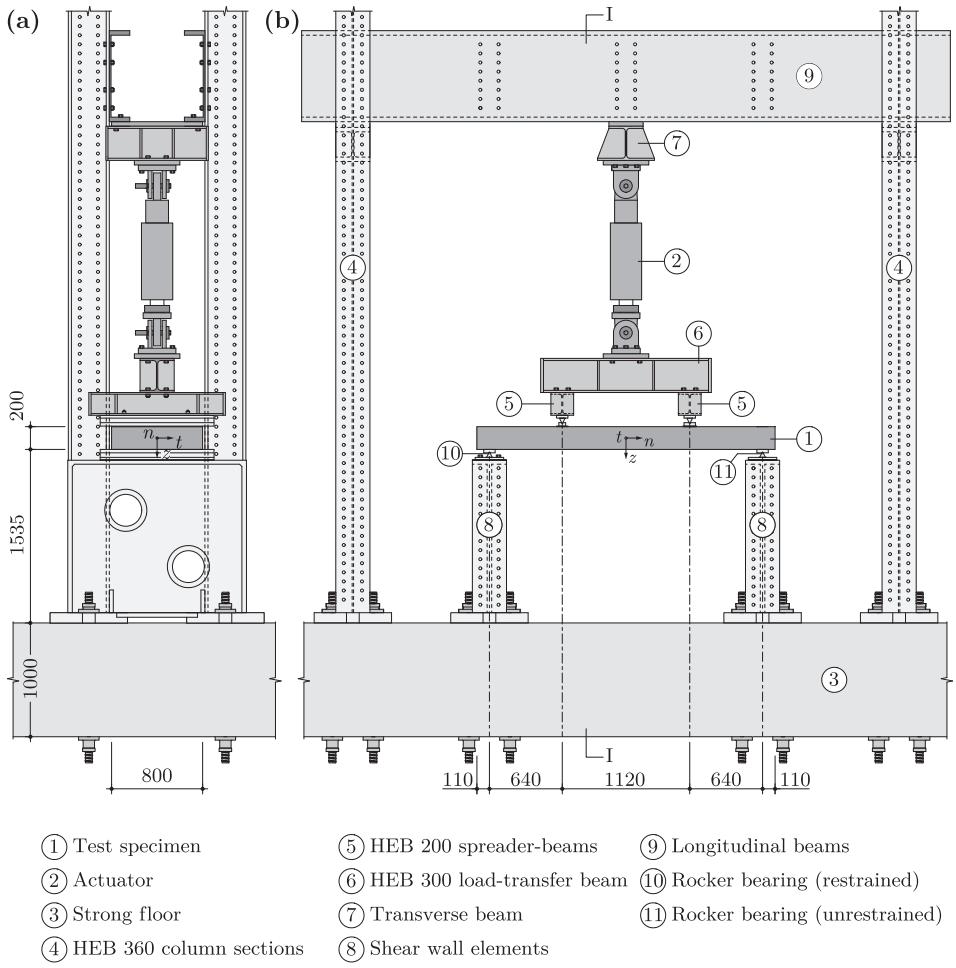

Fig. 3. Test setup: (a) section I-I; (b) front view. Dimensions in mm.

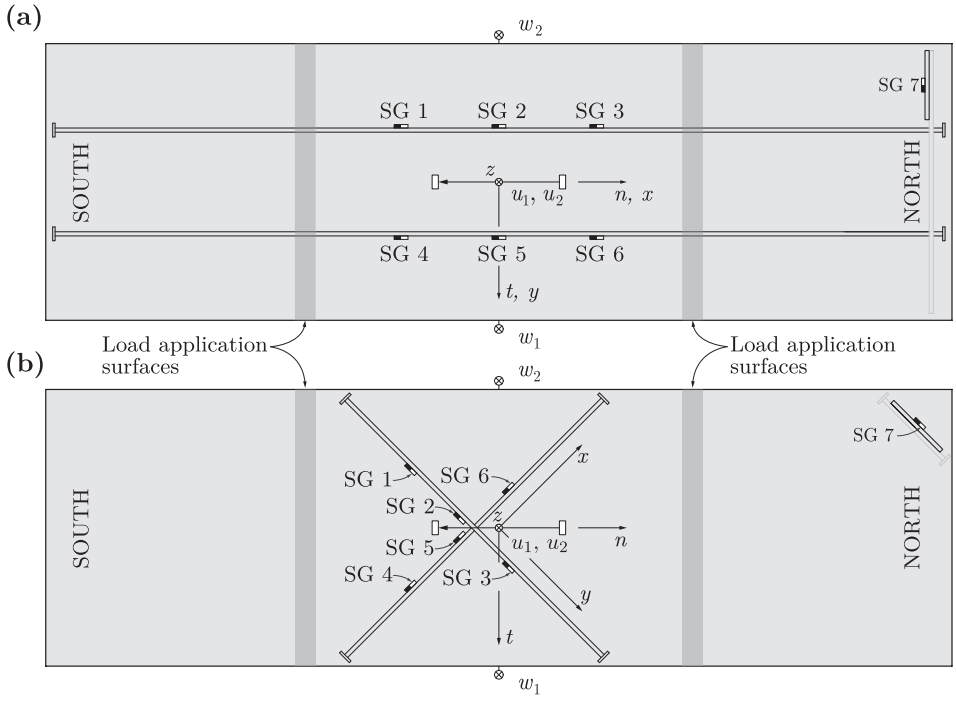

Fig. 4. Plan view layout of permanently installed sensors: (a) series A; (b) series B.

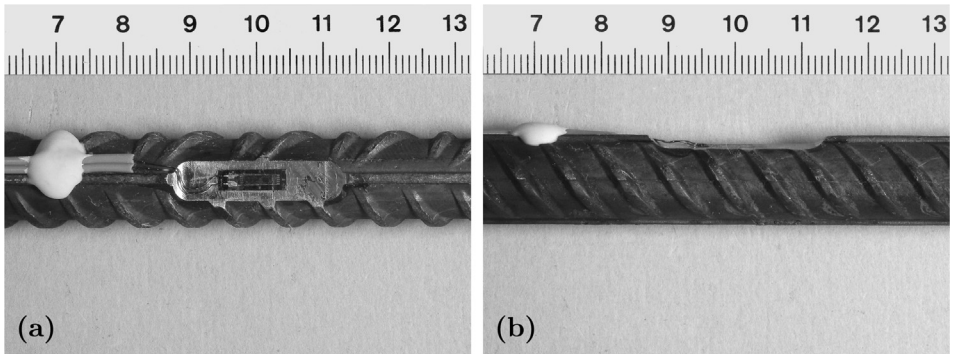

Fig. 5. Reinforcing bar instrumented with a strain gauge: (a) plan view; (b) side view.

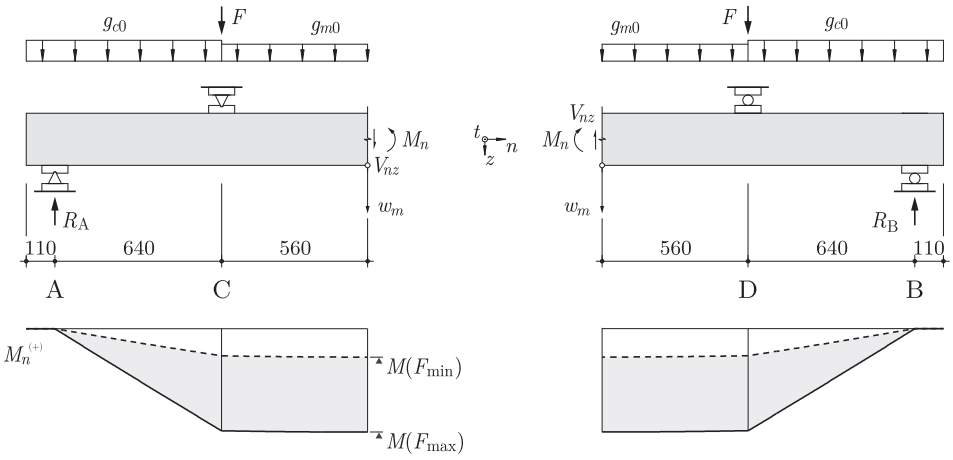

Fig. 6. Static system with relevant forces and distribution of bending moment at maximum and minimum load. Dimensions in mm.

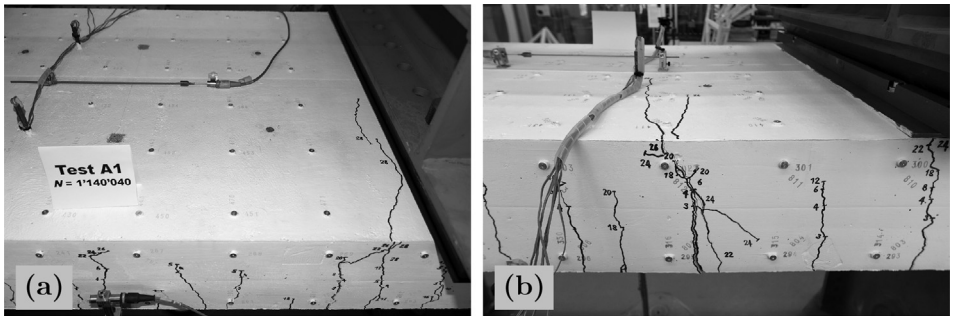

Fig. 7. Critical cross-sections at failure: (a) test A1; (b) test A2.

strain gauge measurements during testing was compensated with a reference measurement. For this purpose, an additional strain gauge SG 7 was applied to a short, identically prepared bar which was cast into an unloaded region of the specimen.

5. Test results

5.1. Analysis and representation of data

The x- and y-axes define the orientation of the outer and inner layers of reinforcement, respectively. The n- and t-directions indicate the longitudinal and transverse axes of the specimen, respectively. Positive forces, displacements and stress resultants are defined as illustrated in Fig. 6. The applied force F [kN] per load application position, the support reactions R [kN] and bending moment at midspan M_n [kN m] were calculated with

$$F = 0.5 \cdot F_{act} + G \tag{1}$$

$$R = 0.75 \cdot g_{c0} + 0.56 \cdot g_{m0} + F \tag{2}$$

$$M_n = 1.2 \cdot R - 0.56 \cdot F - 0.75 \cdot 0.935 \cdot g_{c0} - \frac{1}{2} \cdot 0.56^2 \cdot g_{m0} \tag{3}$$

assuming an equal distribution of force across the loading yoke and support reactions due to symmetry. The weight of the loading yoke and rocker bearings on the top surface of $G = 3.06$ kN per load application position and the own weight of the specimen was considered in the calculations. A specimen weight per unit length was assumed as $g_{c0} = 3.822$ kN/m for the region with shear reinforcement and $g_{m0} = 3.810$ kN/m for the central region without shear reinforcement. The displacement at midspan w_m denotes the mean value of LVDT measurements w_1 and w_2 on the front and back sides of the specimen.

Global *failure* of the specimen constitutes the condition in which the maximum load was no longer reached during quasi-static loading in displacement control. The structural condition upon reaching this criterion was generally characterised by large deflections and often

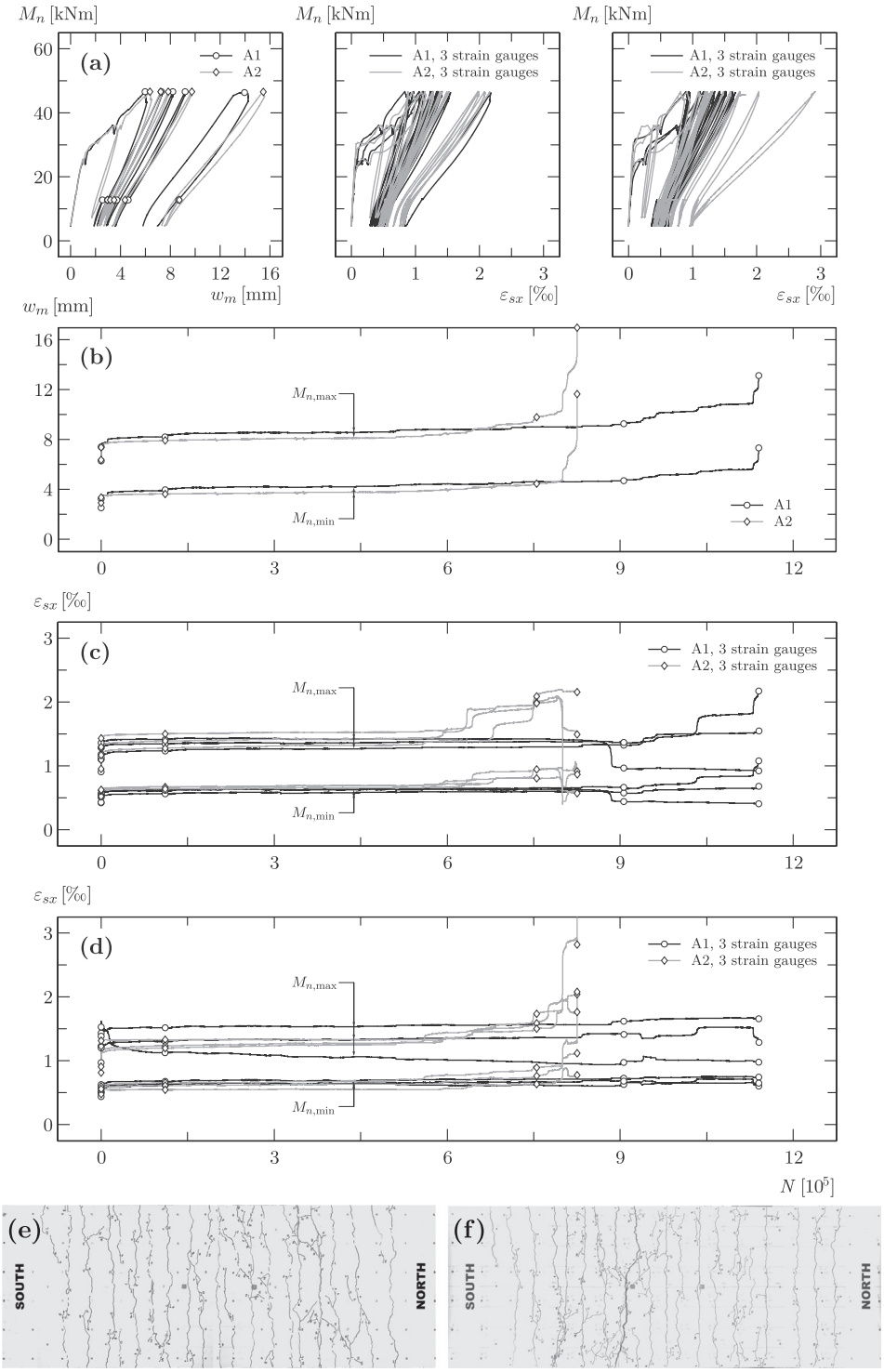

Fig. 8. Series A: (a) moment-deflection and reinforcing steel strains in *x*-direction at selected load cycles; (b) midspan deflection; (c) and (d) reinforcing steel strains in *x*-direction; (e) soffit of test A1 at N_u = 1,140,040; (f) soffit of test A2 at N_u = 825,784.

accompanied by spalling of the cover concrete to the reinforcement. The rupture of reinforcing bars due to large plastic deformations could be heard in most specimens after exceeding the residual flexural resistance.

Reinforcing bar fractures were detected on the basis of measurements with the magnetic flux leakage method. Inspection of the measured signals and comparison with the results from a detection algorithm developed for this purpose resulted in a reliable identification of bar fractures in most cases. Details of this method and more detailed results is provided in the dissertation of *Diederich* [14]. The majority of fractures, and even the onset of fatigue crack formation in some bars, could be detected in the tests of series A. The fracture detection in the tests of series B, however, proved to be less successful with this method; a number of false negative detections were obtained for closely spaced fractures and for fractures within the inner layer of reinforcement. Interpretation of the quasi-continuous measurements of steel strains on the instrumented bars provided a further indication of the rupture of individual bars. The two following characteristics were observed: (1) a

Table 4
Tests A1 and A2: selected measurements at maximum and minimum load for increasing load cycles.

Test A1						Test A2						
N [–]	M_n [kN m]	w_m [mm]	u_1 [mm]	ε_{sx} [‰]	ε_{sy} [‰]	N [–]	M_n [kN m]	w_m [mm]	u_1 [mm]	ε_{sx} [‰]	ε_{sy} [‰]	Level
0	43.06	6.10	−0.21	1.090	–	0	44.14	6.51	−0.27	1.076	–	F_{max}
1	11.99	2.51	−0.08	0.461	–	1	12.98	2.94	−0.11	0.518	–	F_{min}
10	44.33	6.61	−0.22	1.191	–	10	44.82	6.97	−0.29	1.169	–	F_{max}
10	12.35	2.75	−0.09	0.501	–	10	12.95	3.09	−0.11	0.551	–	F_{min}
124	45.22	7.29	−0.24	1.303	–	110	45.18	7.24	−0.29	1.229	–	F_{max}
124	12.27	2.95	−0.09	0.528	–	110	12.87	3.18	−0.12	0.560	–	F_{min}
1,124	45.07	7.55	−0.25	1.322	–	1110	45.78	7.50	−0.30	1.256	–	F_{max}
1,124	12.14	3.13	−0.10	0.542	–	1110	12.94	3.29	−0.12	0.581	–	F_{min}
11,124	46.23	7.78	−0.25	1.345	–	11,110	46.19	7.72	−0.31	1.292	–	F_{max}
11,124	12.16	3.37	−0.10	0.560	–	11,110	12.72	3.37	−0.12	0.591	–	F_{min}
111,133	44.95	8.16	−0.26	1.356	–	111,110	45.78	7.85	−0.32	1.313	–	F_{max}
111,133	12.54	3.68	−0.12	0.591	–	111,110	12.77	3.48	−0.13	0.606	–	F_{min}
311,133	45.30	8.43	−0.27	1.367	–	511,110	45.52	8.05	−0.33	1.343	–	F_{max}
311,133	13.35	4.14	−0.13	0.635	–	511,110	12.96	3.64	−0.14	0.633	–	F_{min}
511,133	45.75	8.62	−0.28	1.387	–	755,347	45.16	9.65	−0.38	1.794	–	F_{max}
511,133	13.16	4.27	−0.14	0.647	–	755,347	12.88	4.28	−0.16	0.817	–	F_{min}
711,133	45.57	8.79	−0.29	1.393	–	800,317	45.10	11.27	−0.43	2.108	–	F_{max}
711,133	13.14	4.47	−0.15	0.659	–	800,317	12.70	5.06	−0.18	0.946	–	F_{min}
906,347	45.28	9.14	−0.29	1.428	–	809,232	45.68	13.00	−0.48	2.191	–	F_{max}
906,347	12.98	4.63	−0.15	0.665	–	809,232	13.05	6.28	−0.22	0.980	–	F_{min}
961,995	45.58	9.83	−0.32	1.471	–	825,514	45.14	15.58	−0.56	2.229	–	F_{max}
961,995	13.27	5.03	−0.17	0.684	–	825,514	12.81	8.66	−0.31	1.363	–	F_{min}
1,035,895	45.55	10.43	−0.33	1.592	–							F_{max}
1,035,895	13.15	5.36	−0.18	0.735	–							F_{min}
1,131,296	45.45	11.41	−0.34	1.627	–							F_{max}
1,131,296	13.27	5.88	−0.18	0.754	–							F_{min}
1,140,040	43.58	14.24	−0.33	1.763	–							F_{max}
1,140,040	13.12	8.60	−0.18	0.846	–							F_{min}

sudden, disproportionally large increase in steel strain indicated failure of a bar other than the one wherein the measurement was made, which was close to or within the cross-section of the measurement position; and (2) a sudden decrease in steel strain indicated rupture of the bar in which the measurement was made. The number of load cycles at which individual bars fractured could be estimated by considering such developments in steel strain as well as the fracture position relative to the strain gauges.

5.2. Tests of series A

Fig. 7 indicates the critical cross-sections in specimens A1 and A2 at failure; the structural response of tests A1 and A2 is illustrated through the continuous measurements at maximum and minimum load in Fig. 8. Selected measurements are summarised in Table 4.

The first reinforcing bar fracture occurred at a greater number of load cycles in test A1 than in A2. The remaining number of load cycles until global failure, however, was similar in both tests. The increase in midspan deflection from the initial loading to the final measurement shortly before failure amounted to 133% and 140% in tests A1 and A2, respectively. The critical cross-section in test A2 developed close to the centre of the test region, see Fig. 7(b). In test A1, the critical crack formed close to a load application surface, i.e. outside the measurement region, see Fig. 7(a). As a result, lower concrete compressive deformations u_1 were measured on the slab top surface in test A1. Reinforcing steel strains were measured at three positions on two bars in x-direction in each specimen, see Fig. 8(c) and (d). Some variation in strain measurements at different locations on the same bar, particularly in the measurements at maximum load, were observed. Such variations can be attributed to the position of the measurement relative to the concrete cracks. High steel strains occur close to the cracks; whereas the activation of bond stresses at the interface between the reinforcing bar and the surrounding concrete results in lower steel strains between adjacent cracks. Large, nearly vertical flexural cracks were observed in both tests at the critical cross-section after the rupture of one or more reinforcing bars. The depth of these cracks increased into the flexural compression zone, subsequently becoming visible in both tests on the top surface of the specimen at failure.

5.3. Tests of series B

Fig. 9 illustrates the structural response of the specimens in series B through the continuous measurements from tests B1 and B2. The critical cross-sections of both tests at failure are shown in Fig. 10. Selected measurements are summarised in Table 5.

The midspan deflection of both tests in series B correlated closely at maximum and minimum load. The ratio of uncracked to cracked stiffness was significantly lower than in the tests of series A due to the deviation between principal moment and reinforcement direction. As a result, the midspan deflection was on average more than 2.5 times greater. The relative increase in midspan deflection between the initial loading and shortly before failure, however, was significantly lower in the tests of series B than in A, amounting to only 74% and 69% in tests B1 and B2, respectively. Concrete deformations on the slab top surface u_1 (compressive) were approximately twice as high as observed in the tests of series A. This indicates high compressive strains within the flexural compression zone in the direction of principal moment. Fig. 9(c) and (d) indicates the development of reinforcing steel strains at maximum and minimum load throughout the fatigue lives of the specimens. These measurements were obtained from three strain gauges on a bar in x-direction and another three on a bar in the y-direction in specimens B1 and B2. The variation in steel strains measured at different points on the same bar was larger than in the tests of series A. Moreover, higher strains were observed on the outer layer of reinforcement in x-direction than those on the inner layer in y-direction. Due to the relatively high level of cyclic loading and after failure of individual bars, the strains in some of the bars shortly before failure were of a magnitude that indicated the onset of yielding of the steel. In

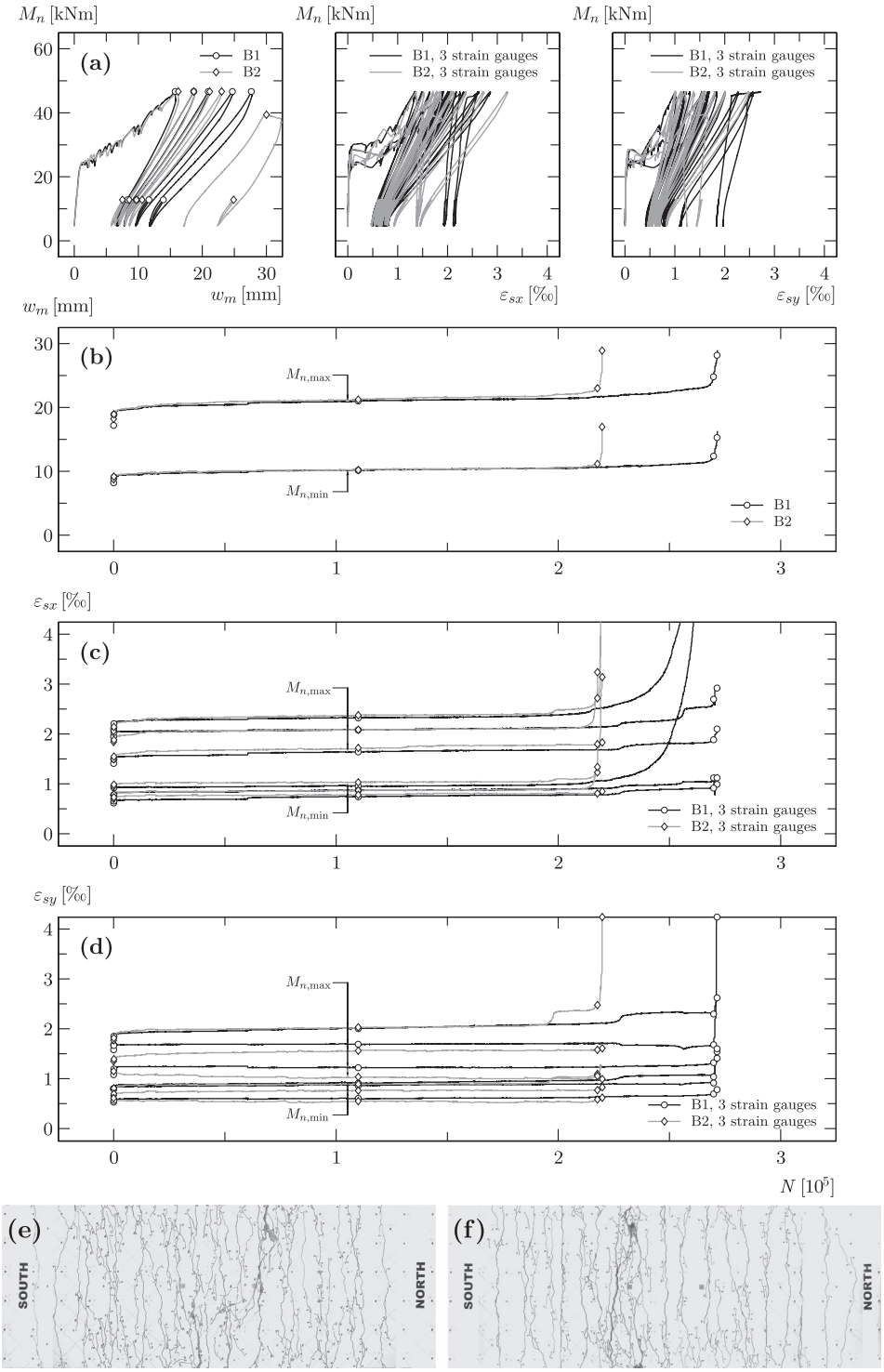

Fig. 9. Series B: (a) moment-deflection and reinforcing steel strains in *x*- and *y*-direction at selected load cycles; (b) midspan deflection; (c) and (d) reinforcing steel strains in *x*- and *y*-direction; (e) soffit of test B1 at N_u = 271,524; (f) soffit of test B2 at N_u = 219,741.

contrast to the transverse cracks observed on the top surfaces of specimens A1 and A2 at failure, cracks with an orientation approximately perpendicular to the direction of the larger principal strain (tension) were observed in test B1, see Fig. 10(a). Such cracks indicate high transverse tensile strains within the flexural compression zone of the specimen. Furthermore, some spalling of the cover concrete to the reinforcement was observed in test B2 at failure. This indicates high compressive strains perpendicular to the larger principal direction within the flexural tensile zone on the slab soffit.

6. Discussion

6.1. Fatigue strength of the reinforcement

Between 8 and 18 fractures were found in each specimen at failure. Multiple fractures were observed in some bars within the test region. Some fractures occurred at short intervals; the minimum distance approximately corresponding to the bar spacing. The sequence of occurrence could partially be derived from the manual and quasi-continuous

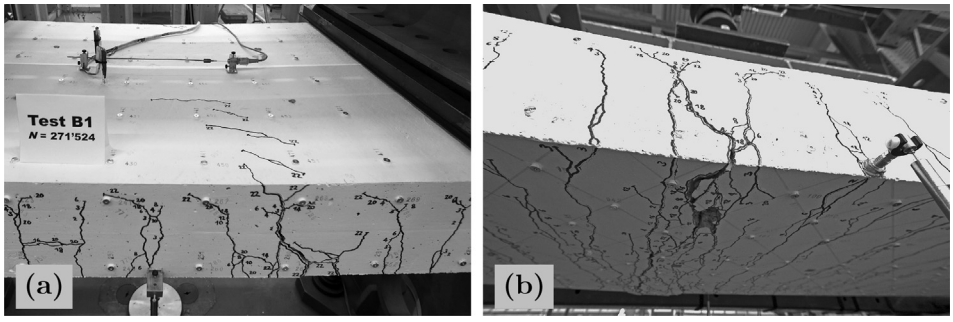

Fig. 10. Critical cross-sections at failure: (a) test B1; (b) test B2.

Table 5
Tests B1 and B2: selected measurements at maximum and minimum load for increasing load cycles.

Test B1						Test B2						
N [–]	M_n [kN m]	w_m [mm]	u_1 [mm]	ε_{sx} [‰]	ε_{sy} [‰]	N [–]	M_n [kN m]	w_m [mm]	u_1 [mm]	ε_{sx} [‰]	ε_{sy} [‰]	Level
0	43.63	15.85	−0.50	1.738	1.392	0	43.54	16.29	−0.47	1.656	1.283	F_{max}
1	13.38	8.06	−0.24	0.790	0.732	1	12.33	7.52	−0.19	0.716	0.600	F_{min}
10	45.09	17.76	−0.54	1.838	1.501	10	44.95	17.89	−0.50	1.773	1.393	F_{max}
10	13.56	8.77	−0.24	0.799	0.743	10	12.57	8.20	−0.20	0.767	0.649	F_{min}
110	45.20	18.74	−0.56	1.872	1.560	110	45.17	18.74	−0.52	1.829	1.432	F_{max}
110	12.43	8.33	−0.22	0.738	0.687	110	12.84	8.65	−0.21	0.790	0.666	F_{min}
1,110	45.65	19.36	−0.58	1.919	1.594	1110	45.37	19.36	−0.54	1.887	1.455	F_{max}
1,110	12.66	8.72	–	0.765	0.713	1110	12.65	8.86	−0.22	0.800	0.668	F_{min}
11,110	45.57	19.79	−0.59	1.940	1.612	11,110	46.08	20.09	−0.56	1.972	1.500	F_{max}
11,110	12.71	9.01	−0.25	0.780	0.726	11,110	12.60	9.04	−0.23	0.830	0.688	F_{min}
60,278	45.64	20.56	−0.61	1.965	1.635	110,000	45.94	21.16	−0.59	2.048	1.521	F_{max}
60,278	12.40	9.29	−0.26	0.782	0.731	110,000	12.84	9.72	−0.25	0.861	0.709	F_{min}
110,000	46.00	20.98	−0.62	2.010	1.848	217,555	46.11	23.08	−0.63	2.577	1.691	F_{max}
110,000	12.95	9.74	−0.27	0.825	0.843	217,555	12.64	10.59	−0.27	1.199	0.774	F_{min}
269,807	45.70	24.70	−0.71	2.241	1.969	219,079	45.64	24.60	−0.65	3.082	1.766	F_{max}
269,807	12.88	11.65	−0.32	1.280	0.919	s219,079	12.46	11.24	−0.27	1.700	0.796	F_{min}
271,345	45.26	27.74	−0.89	2.460	2.349	219,728	45.23	27.48	−0.68	–	–	F_{max}
271,345	12.81	13.91	−0.42	1.339	1.556	219,728	12.68	14.36	−0.31	–	–	F_{min}
						219,741	36.79	32.31	−0.66	–	–	F_{max}
						219,741	12.67	24.87	−0.37	–	–	F_{min}

Table 6
Sequence of reinforcing bar fractures for tests A1 and A2.

Test A1			Test A2		
Fracture no.	N_u [a,b]	Type	Fracture no.	N_u [a,b]	Type
103	(834,100)	Fatigue	207	(560,200)	Fatigue
111	(885,000)	Fatigue	209	(592,900)	Fatigue
110	906,347	Fatigue	215	(634,100)	Fatigue
102	(940,600)	Fatigue	214	(643,800)	Fatigue
106	(958,700)	Fatigue	216	(680,200)	Fatigue
105	961,995	Fatigue	211	(748,600)	Fatigue
108	(1,033,200)	Fatigue	204, 206, 208, 213	755,347	Fatigue
101	1,035,895	Fatigue	205	(790,100)	Fatigue
107, 109	1,131,296	Fatigue	201, 202	800,317	Fatigue
104	1,140,040	Fatigue-ductile	212	(800,500)	Fatigue
			210, 217	809,232	Fatigue
			203	825,514	Fatigue
			218	825,784	Ductile

[a] The load cycle at failure is based on the detection with the magnetic flux leakage method.
[b] Values in brackets indicate an estimation from strain measurements.

Table 7
Sequence of reinforcing bar fractures for tests B1 and B2.

Test B1			Test B2		
Fracture no.	N_u [a,b]	Type	Fracture no.	N_u [a,b]	Type
303	(214,400)	Fatigue	406, 407	(197,900)	Fatigue
307	(227,900)	Fatigue	402	(216,500)	Fatigue (SG 5)
301, 308, 310, 311	269,807	Fatigue	401, 403	219,079	Fatigue
304, 309, 312, 313	271,345	Fatigue	404, 408	219,741	Fatigue
306	271,345	Fatigue (SG 6)	405	219,741	Fatigue
305	271,524	Fatigue			
302	271,524	Fatigue-ductile			

[a] The load cycle at failure is based on the detection with the magnetic flux leakage method.
[b] Values in brackets indicate an estimation from strain measurements.

measurements. The occurrence of reinforcing bar fractures in the tests of series A and B is summarised in Tables 6 and 7, respectively. Moreover, a characterisation of fracture type is indicated as either “fatigue” or “ductile” on the basis of an inspection of the fracture surface.

Calculations with a model developed by the first author [15] and interpretation of the reinforcing steel strain measurements, as presented in [16], enable a prediction of the stress range in the reinforcement under cyclic loading. The proposed model makes use of a layered element formulation and incorporates approaches such as the *Cracked*

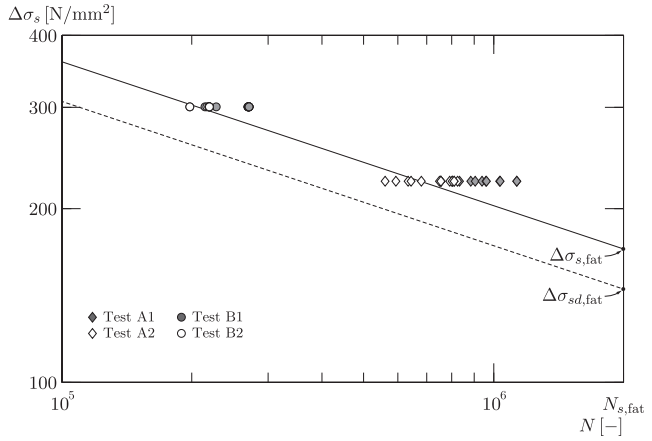

Fig. 11. Fatigue fracture of reinforcing steel bars in the tests of series A and B.

Membrane Model [17], previously developed at the Institute of Structural Engineering of ETH Zurich for quasi-static loading conditions, in order to realistically predict reinforcing steel stresses at the concrete cracks. For the tests of series A, the model prediction of reinforcing steel stress range amounts to $\Delta\sigma_s = 223$ N/mm^2 between the maximum and minimum load levels. The finite width of the slab strip specimens, however, results in a variable reinforcement content within the constant moment region in the tests of series B. The effective reinforcement content is lower than in the tests of series A; thus, resulting in higher reinforcing steel stresses for the tests of series B. The calculations indicate a stress range of $\Delta\sigma_s = 300.5$ N/mm^2 for both the x- and y-directions of reinforcement. Fig. 11 indicates the number of load cycles at which bar fractures were detected in the tests of series A and B at the corresponding stress range in double logarithmic form. This representation of the results constitutes an S-N diagram of the individual fractures in all four test specimens. The fatigue strength curve for the finite-life region is indicated for both the nominal fatigue strength $\Delta\sigma_{s,\text{fat}}$ (continuous line) and the design value $\Delta\sigma_{sd,\text{fat}}$ (dashed line) recommended in the Swiss standard [18,19].

All fractures occurred at a greater number of load cycles than indicated by the design fatigue strength curve. In both series of tests, however, a number of fractures occurred at less load cycles than indicated by the curve representing the nominal fatigue strength. The first fractures in tests A1 and A2 occurred at $N = 834{,}100$ and 560,200, whereas global failure occurred at $N_u = 1{,}140{,}040$ and 825,784 load cycles, respectively. In other words, the first fatigue fracture occurred at 73% and 68% of the total number of load cycles until failure in tests A1 and A2, respectively. In tests B1 and B2, first fractures were detected at approximately $N = 214{,}400$ and 197,900 load cycles, respectively. Global failure occurred in test B1 at $N_u = 271{,}524$ and in test B2 at 219,741 load cycles. Hence, the first fatigue fracture in tests B1 and B2 occurred at 79% and 90% of the total number of load cycles to global failure, respectively.

6.2. Reinforcing bars inclined to crack direction

Flexural cracks in reinforced concrete slabs initially form perpendicular to the direction of principal moment. Where the principal moment and reinforcement directions coincide, i.e. uniaxial or biaxial bending, the cracks form perpendicular to the reinforcement direction, see Fig. 12(a). Such bars may be assumed to be subjected to purely uniaxial loading. In slab regions subjected to high torsional moments, the direction of principal moment deviates from the reinforcement direction. The orientation of flexural cracks is no longer perpendicular to the reinforcement direction. Considering the geometric compatibility of a crack opening requires such bars to undergo a reorientation in a direction normal to the crack [20], see Fig. 12(b). High loads will result in local crushing of the concrete at the inner surface of the bar; thus, allowing only a partial reorientation. The reinforcing bars in such regions experience a local bending and/or possibly shear action in addition to axial tensile loading. Tests have indicated that such a reorientation of bars at the cracks has little influence on the ultimate resistance of slabs [20]. Fatigue, however, occurs under service conditions; typically at significantly lower stress levels than the ultimate strength.

The fracture pattern of reinforcing bars adjacent to the critical crack observed in test B2 suggests some degree of reorientation, see Fig. 13. Bar fractures occurred within both the outer and inner layer of reinforcement. The fractures denoted by No. 406 and 407 occurred in the same bar within the inner layer of reinforcement at a distance corresponding roughly to the bar spacing. Furthermore, the fracture surfaces on both sides of the critical crack indicate some misalignment due to the opening of the crack at an inclination to the bar direction, see Fig. 13(b).

All fractures in the tests of series B occurred at significantly fewer load cycles than those in the tests of series A. Global failure occurred in tests B1 and B2 on average at only 25% of the number of load cycles sustained in tests A1 and A2. The lower fatigue lives, however, can be attributed to the higher reinforcing steel stress range observed in the tests of series B. Considering the S-N diagram of bar fractures shown in Fig. 11, the reduced number of load cycles to failure observed in the tests of series B is appropriately reflected in the fatigue strength curve. The tests therefore indicate that an inclination of reinforcing bars with respect to the direction of principal stress – even at levels of applied cyclic loading exceeding typical service conditions – does not

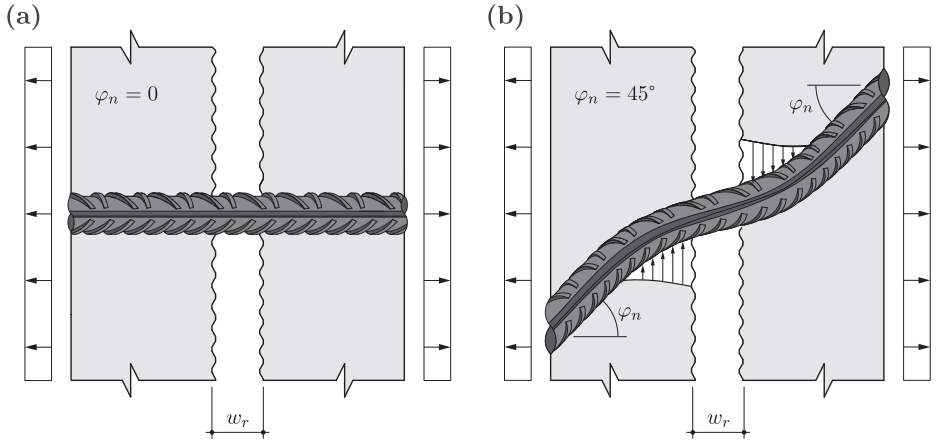

Fig. 12. Reinforcing bar orientation relative to concrete cracks: (a) perpendicular to cracks; (b) inclined with respect to cracks, adapted from [20]. Note: the crack width is exaggerated.

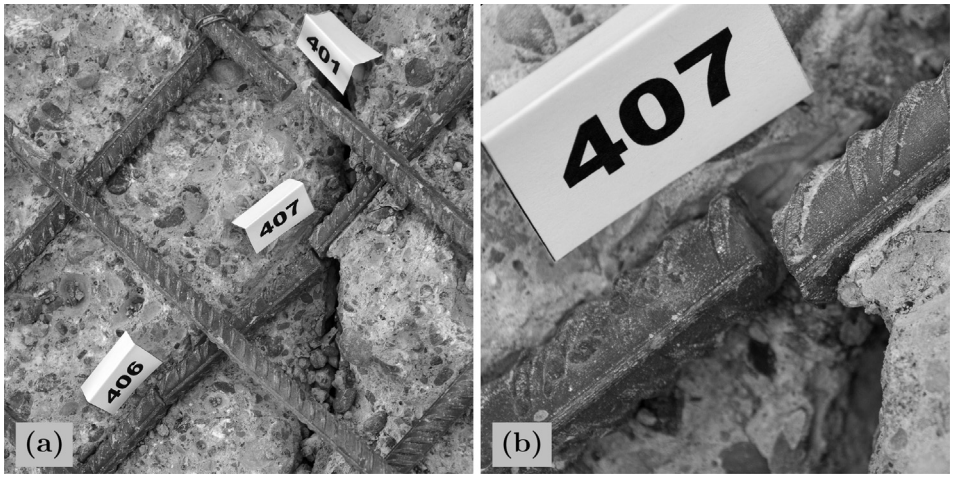

Fig. 13. Exposed bar fractures in test B2: (a) overview at critical cross-section; (b) detail of fracture No. 407 across the critical crack.

detrimentally affect their fatigue strength.

7. Conclusions

The present experimental campaign was carried out to investigate the fatigue performance of orthogonally reinforced concrete slabs wherein the principal moment and reinforcement direction do not coincide. On the basis of the experimental results, a number of conclusions could be drawn with regards to the load-carrying behaviour of slabs under high levels of cyclic loading. The main conclusions can be summarised as follows:

7.1. General

Fatigue represents a realistic hazard scenario for reinforced concrete slabs with a typical reinforcement content. For predominant bending action, a relatively gradual but continuous deterioration of the load-deformation behaviour is observed. Measurable changes in structural response occur upon failure of individual bars; especially pronounced were the increases in reinforcing steel strains. A detailed inspection of the exposed bar fractures in all four tests indicate that the local milling of the instrumented bars along the longitudinal rib, as indicated in Fig. 5, was not significantly detrimental for the fatigue properties. Out of a total of 50 bar fractures, only two occurred within the milled regions. Changes in the concrete deformations on the slab top surface and soffit were also observed upon reinforcement rupture. The occurrence of bar failures was characterised by localisations of concrete strains and curvatures in the critical cross-sections. Furthermore, local increases in crack widths were observed in the proximity of bar fractures as well as the formation of secondary cracks in some cases. Global failure in bending occurs when the residual flexural strength, following rupture of individual reinforcing bars, falls below the bending demand. Such a mode of failure was observed in all four tests.

7.2. Reinforcing bars inclined to crack direction

The four tests were performed at high levels of reinforcing steel stress range that exceed the expected range of approximately 100–150 N/mm^2 under typical service conditions in bridge deck slabs. A generalised interpretation of the results presented in this paper, especially within the *long-life* fatigue region, is therefore limited. By directly comparing the reinforcement fatigue strengths observed in the two series of tests, however, some insight is gained into the differences in fatigue performance with respect to the reinforcement orientation. An evaluation of reinforcing steel strain measurements indicates higher stress ranges in the tests of series B than in series A. As a result, tests B1 and B2 failed on average at only 25% of the total number of load cycles observed for tests A1 and A2. The number of load cycles corresponding to bar fractures at the expected stress ranges in the tests of both series correlate well with the fatigue strength curve in an S-N diagram representation. The fatigue strength of the tests in series B can therefore be evaluated as being similar to the tests in series A. Hence, the tests indicate that the fatigue strength of bars inclined with respect to the direction of principal stress is comparable to that of bars orientated in the principal stress direction.

7.3. Redistribution of internal forces

Measurements of reinforcing steel strains during cyclic loading indicate sudden, disproportionally large increases that correspond to the fracture of individual bars. Moreover, the failure of a bar in one layer of reinforcement in the tests of series B was observed as an increase in steel strains on the other, perpendicularly orientated layer activated in bending. This confirms that a redistribution of internal forces occurs under cyclic loading upon rupture of individual bars. Such a redistribution may even extend to other layers of reinforcement activated in bending.

7.4. Remaining service life after first fatigue damage

Failure of a single reinforcing bar in members reinforced with multiple bars generally does not signify immediate collapse. Slabs are typically reinforced with layers of closely spaced bars. Their structural behaviour is relatively insensitive to the failure of single bars. The *remaining fatigue life*, defined by *Fehlmann* [7] as the phase after failure of the first bar until global failure of the structural member, amounted on average to 29% and 15% of the total fatigue life for the tests in series A and B, respectively. A significant increase in the remaining fatigue life could be expected at lower levels of cyclic loading more closely resembling the typical service conditions in bridge deck slabs. The progressive deterioration of load-carrying capacity associated with fatigue fracture of individual bars in the present tests was characterised by sudden, disproportionally large increases in deflection as well as in the widths of existing cracks, possibly localised formation of secondary cracks and/or spalling of the cover concrete to the reinforcement. The identification of these characteristics in existing concrete structures could serve as warning signals for the potential onset of fatigue damage.

Acknowledgements

The authors gratefully acknowledge the financial support provided by the Association of the Swiss Cement Industry *cemsuisse*, Project No.

201305. We are also grateful towards Ancotech AG for sponsoring the reinforcing steel for the experimental work.

References

[1] Balázs GL. Fatigue of bond. ACI Mater J 1991;88(6):620–9.
[2] Tilly GP, Owen DG, Molzahn R, et al. Fatigue of concrete structures, state-of-the-art-report. Bulletin d' Information No. 188. Dubrovnik: Comité Euro-International du Béton; 1988.
[3] Schläfli M, Brühwiler E. Fatigue of existing reinforced concrete bridge deck slabs. Eng Struct 1998;20(11):991–8.
[4] Johansson U. Fatigue tests and analysis of reinforced concrete bridge deck models. Dissertation. Stockholm: Royal Institute of Technology; 2004.
[5] Schläfli M. Ermüdung von Brückenfahrbahnplatten aus Stahlbeton (Fatigue of reinforced concrete bridge deck slabs). Dissertation No. 1998. EPF Lausanne; 1999.
[6] Zanuy C, Maya LF, Albajar L, de la Fuente P. Transverse fatigue behaviour of lightly reinforced concrete bridge decks. Eng Struct 2011;33(10):2839–49.
[7] Fehlmann P. Zur Ermüdung von Stahlbetonbrücken (on fatigue of structural concrete bridges). Dissertation No. 20231. ETH Zurich; 2012.
[8] Schweizerischer Ingenieur- und Architektenverein (SIA). Norm SIA 261(2003) Einwirkungen auf Tragwerke (Actions on structures). Zürich; 2003.
[9] Chang TS, Kesler CE. Static and fatigue strength in shear of beams with tensile reinforcement. ACI J Proc 1958;54(6):1033–57.
[10] Brühwiler E, Hajdin R, Kunz P. Fatigue safety of existing concrete bridges in Jeopardy? In: Developments in short and medium span bridge engineering '94. The Canadian Society for Civil Engineering; 1994. p. 1209–17.
[11] Grünberg J, Hansen M, Liebig JP. Ermüdungsbeanspruchungen von Betonbrücken unter zunehmendem Schwerverkehr (Fatigue action in concrete bridges under increasing traffic loads). Beton- und Stahlbetonbau 2007;102(9):596–606.
[12] Jäger T, Marti P. Reinforced concrete slab shear prediction competition: experiments. ACI Struct J 2009;106–S29:300–8.
[13] Ancotech AG. ancoFIX®– Bewehrungen, Ancotech AG, Dielsdorf, Schweiz; 2013.
[14] Diederich H. Zerstörungsfreie Prüfung der Bewehrung von Betonbauteilen mithilfe der Magnetischen Streufeldmethode (Nondestructive testing of the reinforcement of structural concrete elements with the magnetic flux leakage method). Dissertation No. 23733, ETH Zurich; 2016.
[15] Spathelf CA. Fatigue performance of orthogonally reinforced concrete slabs. Dissertation no. 24515. ETH Zurich; 2017.
[16] Spathelf CA, Vogel T. Experimentelle Untersuchung zum Ermüdungsverhalten von kreuzweise bewehrten Stahlbetonplatten (Experimental investigation on the fatigue performance of orthogonally reinforced concrete slabs), cemsuisse-Projekt 2011305 – Juni 2017. Institut für Baustatik und Konstruktion, ETH Zürich; 2017.
[17] Kaufmann W, Marti P. Structural concrete: cracked membrane model. ASCE J Struct Eng 1998;124(12):1467–75.
[18] Schweizerischer Ingenieur- und Architektenverein (SIA). Ermüdung von Betonbauten (Fatigue of concrete structures). SIA Dokumentation D 0133, Zürich; 1997.
[19] Schweizerischer Ingenieur- und Architektenverein (SIA). Norm SIA 262(2013) Betonbau (Concrete construction). Zürich; 2013.
[20] Lenschow RJ, Sozen MA. A yield criterion for reinforced concrete under biaxial moments and forces. Structural research series no. 311. University of Illinois; 1966.